Optimized compressive sampling for passive millimeter-wave imaging

Leonidas Spinoulas,[1,*] Jin Qi,[2] Aggelos K. Katsaggelos,[1] Thomas W. Elmer,[3] Nachappa Gopalsami,[3] and Apostolos C. Raptis[3]

[1]Department of Electrical Engineering and Computer Science, Northwestern University, 2145 Sheridan Road, Evanston, Illinois 60208, USA

[2]Department of Electrical Engineering, University of Electronic Science and Technology of China, 2006 Xiyuan Avenue, Gaoxin District, Chengdu 611731, China

[3]Argonne National Laboratory, Nuclear Engineering Division, Bldg. 308, 9700 S. Cass Avenue, Lemont, Illinois 60439-4825, USA

*Corresponding author: leonidasspinoulas2015@u.northwestern.edu

Received 29 June 2012; revised 9 August 2012; accepted 13 August 2012; posted 14 August 2012 (Doc. ID 171652); published 7 September 2012

In this paper, we briefly describe a single detector passive millimeter-wave imaging system, which has been previously presented. The system uses a cyclic sensing matrix to acquire incoherent measurements of the observed scene and then reconstructs the image using a Bayesian approach. The cyclic nature of the sensing matrix allows for the design of a single unified and compact mask that provides all the required random masks in a convenient way, such that no mechanical mask exchange is needed. Based on this setup, we primarily propose the optimal adaptive selection of sampling submasks out of the full cyclic mask to obtain improved reconstruction results. The reconstructed images show the feasibility of the imaging system as well as its improved performance through the proposed sampling scheme.

OCIS codes: 110.0110, 110.1085, 100.3010, 100.3190, 110.1758, 280.4991.

1. Introduction

The millimeter-wave (MMW) regime lies in the microwave spectrum in the frequency band between 30 and 300 GHz. All natural objects, whose temperature is above absolute zero, emit passive MMW radiation. Passive millimeter-wave imaging (PMMWI) offers significant advantages over optical visible light and infrared imaging. In poor weather conditions such as fog, snow, rain, clouds, smoke, and dust, PMMW radiation is attenuated multiple orders of magnitude less than visual or infrared radiation [1]. Furthermore, PMMWI can function during both day and night. The amount of radiation emitted in the MMW regime is 10^8 times smaller than the amount emitted in the infrared one. However, current MMW receivers have at least 10^5 times better noise performance, while the temperature contrast recovers the remaining 10^3. This makes MMW imaging comparable in performance with current infrared systems [2]. The ability to capture radiation in low-visibility conditions has led to numerous applications of MMW technology over the years [1]. These applications are relevant to homeland security, aeronautics, diagnostics, defense, and environment science. Recently, active and passive MMW scanners have been successfully used in airports to detect a broad range of concealed threats [3].

Unfortunately, current PMMWI systems suffer from several limitations in terms of the tradeoff between signal-to-noise ratio (SNR) and acquisition time. Two main types of imaging systems are commonly used. Single radiometer imaging systems use

1559-128X/12/266335-08$15.00/0

raster scanning (moving the radiometer or a lens in front of the radiometer), while real-time imaging applications utilize focal-plane radiometer arrays to acquire the whole image. The former systems exhibit low acquisition speeds, while the latter tend to have high complexity and operational cost [4].

Often, costs are mitigated in PMMWI systems by employing only a single radiometer. To retain this cost benefit while minimizing acquisition time, one can incorporate compressive sensing (CS) techniques. CS has become a fast growing field in recent years due to its interesting theoretical nature and its potential aid in numerous practical applications [5,6]. CS uses a small number of random incoherent linear projections of a signal (e.g., an image) and tries to obtain the original signal through a reconstruction algorithm. It is basically an efficient sampling scheme, which overpasses the Shannon sampling theorem limit, exploiting the sparsity inherent in many signals (e.g., natural images, PMMW images). Thus, it enables the reduction of required samples, minimizing the long-acquisition time of a full raster scan of the scene through a single radiometer while still providing comparable imaging quality.

The first prototype of a CS imaging system for visible light applications was presented in [4], while different setups, such as the one presented in [7], have also been proposed. Recently, a more compact form of a single-pixel camera, based on the same principles and tailored for commercial use, was described in [8]. For an overview of optical architectures for compressive imaging, see [9]. In the MMW spectrum, CS has been applied successfully for a few different imaging applications [10–13], namely holography, PMMW imaging with extended depth of field, and sub-MMW imaging.

In this paper, we describe a single radiometer PMMWI system based on Bayesian CS and we propose an efficient and adaptive sampling scheme for improved reconstruction quality. The main advantage of our system, compared to existing ones, [12,13], is its simple design, which is based on conventional imaging principles.

2. Compressive Sensing Passive Millimeter-Wave Imaging System

The proposed PMMW imager, which has been previously presented in [14,15], is depicted in Fig. 1. It shows a single radiometer PMMW setup for CS imaging. To collect incoherent measurements, an extended binary mask is raster scanned in front of the scene using a two-dimensional (2D) controller, and the illuminated radiation through a part of it (submask) is collected by a 2.54 cm diameter dielectric lens and fed to a 146–154 GHz Dicke-switched radiometer [14,15]. The mask is used to multiply the radiation at different locations with 0 or 1, and the collection lens works effectively as an integrator. Combined, these two elements implement an inner product of the incident radiation with a submask configuration. The usage of masks to obtain incoherent

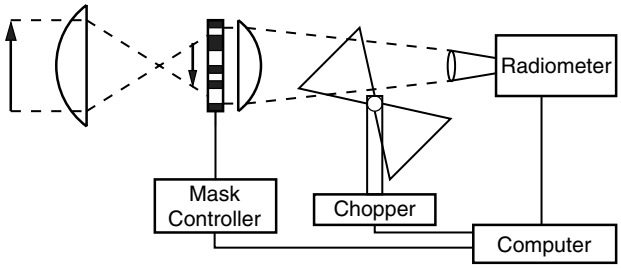

Fig. 1. Schematic of the CS PMMW imager, previously presented in [14,15].

CS measurements has also been proposed in [16] for a terahertz (THz) imaging system, which uses a total of 600 different random masks. Moreover, a time-efficient and cost-effective mask design for this system, based on Toeplitz matrices, has been provided in [17]. Compared to these methods, our proposed mask offers a much more compact design, suitable for minimizing the volume and weight of the CS PMMW imager.

Mathematically, we can express a single radiometer measurement y_i as

$$y_i = \Phi_i \mathbf{x} + n_i, \tag{1}$$

where the row vector Φ_i of length N represents an ordered submask configuration. Vector $\mathbf{x}$ $(N \times 1)$ represents the lexicographically ordered unknown image, and n_i is the acquisition noise. The image $\mathbf{x}$ and each submask configuration are assumed to contain $N = p \times q$ pixels. The acquisition of all possible N measurements with different submask configurations can then be expressed as

$$\mathbf{y} = \Phi \mathbf{x} + \mathbf{n}, \tag{2}$$

where $\mathbf{y}$ is the observation vector of size $N \times 1$ and Φ is the measurement matrix constructed by concatenating all possible N Φ_i's, resulting in a size of $N \times N$.

The compressed acquisition equation of M measurements $(M \ll N)$ is equivalently

$$\mathbf{y}_M = \Phi_M \mathbf{x} + \mathbf{n}_M. \tag{3}$$

3. Mask Construction

In the aforementioned PMMWI system, the measurement matrix Φ corresponds to the mask reported in the schematic of Fig. 1. This mask constitutes a cyclic S-matrix [18], which is closely related to a Hadamard matrix. The definition of an S-matrix follows. Suppose H_n is a normalized Hadamard matrix of order n (meaning that its first row and column contain all 1's). Then let S or S_{n-1} be the $(n-1) \times (n-1)$ matrix of 0's and 1's obtained by omitting the first row and column of H_n and then changing the 1's to 0's and the −1's to 1's. The rows of an S-matrix are pseudo-random sequences, or codewords in a *simplex* code (hence the name). For optical applications, it is most

convenient if the S-matrix is a cyclic or left circulant matrix, i.e., has the property that each row is obtained by shifting the previous row by one to the left. This considerably reduces the cost of the optical apparatus, since N individual masks, of N slits each, can be replaced by a single mask in a compact form, as we will explain.

S-matrices share many common properties with uniformly redundant arrays (URAs) [19,20], and they actually constitute a subset of URAs. URAs have been studied extensively in the past due to their high throughput and low noise effects in coded aperture imaging, and many different compact forms (linear, rectangular, hexagonal) have been proposed. The interested reader is referred to [21] for an extensive overview.

Figure 2 shows the relationship between the full cyclic S-matrix Φ as well as its correspondence to the real mask and its submasks being used for each acquisition. The cyclic nature of the matrix allows for the use of a single extended 2D mask of size $(2p-1)\times(2q-1)$ to expose a $p\times q$ submask for each acquisition by raster scanning the large mask one pixel at a time. Hence, the actual full size mask of size $(2p-1)\times(2q-1)$ allows for all possible N acquisitions when different $p\times q$ regions of the mask are chosen. Clearly, for CS, we are interested in choosing only M out of all possible N submasks, which correspond to M lines of the S-cyclic matrix Φ or M different $p\times q$ regions of the real mask (example regions are highlighted on the real mask at the bottom-right of Fig. 2).

We first construct a cyclic S-matrix of size $N\times N$ using the twin prime construction [18]. This construction produces cyclic S-matrices of order N whenever $N=p(p+2)$ and both p and $q=p+2$ are prime numbers. This gives S-matrices of orders 15, 35, 143, 323, 899, 1763, 3599, etc. Following, we rearrange the elements of the first row of the S-matrix into a $p\times q$ configuration. The large acquisition mask (real mask) is then obtained by periodically repeating the $p\times q$ matrix and retaining a matrix of size $(2p-1)\times(2q-1)$, as illustrated in Fig. 2. We use $N=1763$ with $p=41$ and $q=43$ and a pixel size of 1.24 mm to produce a 10.04 cm × 10.53 cm extended mask with $(2p-1)\times(2q-1)=81\times 85$ pixels. The mask was fabricated using chrome coating on a MMW transparent quartz plate at Argonne National Laboratory (ANL) [14,15].

The one-to-one correspondence between the rows of the S-cyclic matrix and the $p\times q$ subregions of the real mask might not be obvious at first glance. Therefore, we provide an example for an S-cyclic matrix of order $N=35$, which can be represented in a $p\times q=5\times 7$ configuration, in Fig. 3. It is apparent that sliding the selected submask over the extended $(2p-1)\times(2q-1)=9\times 13$ mask is equivalent to cyclic shifts of the first mask (highlighted with a black rectangle), which corresponds to the first row of the S-cyclic matrix, as presented in Fig. 2. Hence, moving the full 2D mask in front of the scene, one pixel horizontally or vertically at a time, allows for the selection of $N=35$ different submasks.

4. Image Reconstruction and Proposed Sampling Scheme

Using CS, we acquire a much smaller number of measurements than the number of pixels in the image, i.e., $M\ll N$, and can still reconstruct the observed scene through a Bayesian CS reconstruction method. The Bayesian method utilized here has been previously investigated [14,22], and its details will be omitted.

The algorithm is based on the fact that PMMW images contain very little texture, and the edge structure is much simpler than in natural images, allowing them to have highly sparse representations [14]. Using this observation, it can be assumed that high-pass filtering of the image $\mathbf{x}$ produces an image with most pixels zero or negligibly small such that the high-pass filtered image is sparse in the spatial domain. This is modeled by placing a sparsity-inducing Gaussian prior on each pixel in the high-pass filtered image. Mathematically, this is expressed as

$$p(\mathbf{x}|\mathbf{A}_k)\propto\left|\sum_{k=1}^{L}\mathbf{D}_k^T\mathbf{A}_k\mathbf{D}_k\right|^{\frac{1}{2}}\exp\left(-\frac{1}{2}\sum_{k=1}^{L}\mathbf{x}^T\mathbf{D}_k^T\mathbf{A}_k\mathbf{D}_k\mathbf{x}\right), \tag{4}$$

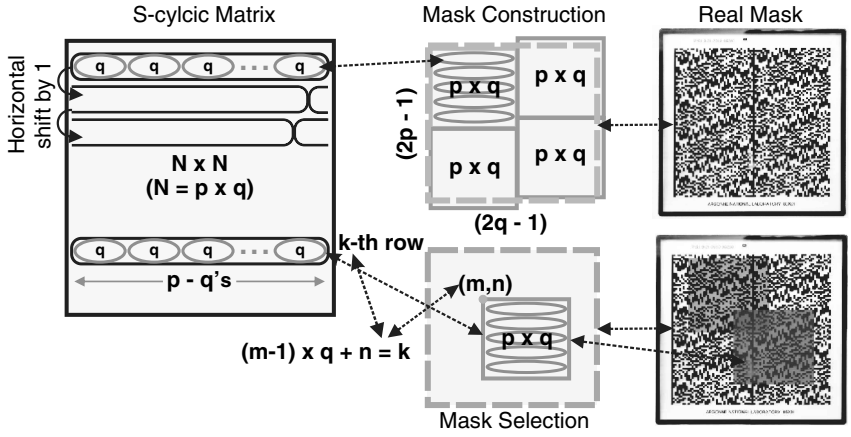

Fig. 2. Mask construction—correspondence between the S-cyclic matrix and the real mask.

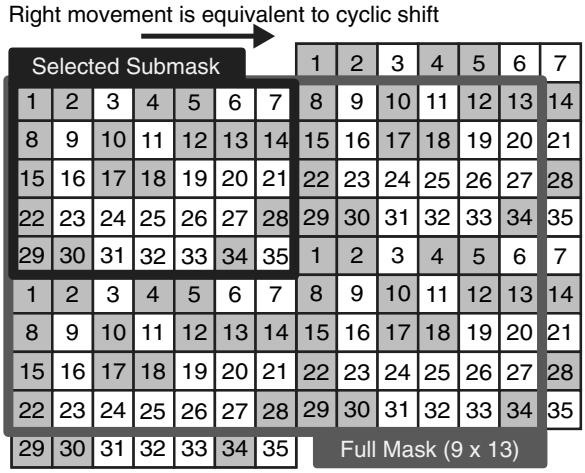

Fig. 3. Example of an S-cyclic matrix of order $N = 35$ rearranged in a $p \times q = 5 \times 7$ configuration and giving rise to a $(2p-1)\times(2q-1) = 9 \times 13$ full mask. The gray and white squares correspond to opaque (0's) and transparent (1's) elements, respectively.

where $\mathbf{D}_k$, $k = 1, 2, \ldots, L$ are $N \times N$ high-pass filters, and $\mathbf{A}_k$ are diagonal precision matrices corresponding to each filter output $\mathbf{D}_k\mathbf{x}$ with $\mathbf{A}_k = \mathrm{diag}(\alpha_{ki})$, $i = 1, \ldots, N$.

Adopting a hierarchical Bayesian framework and using the white Gaussian noise assumption for the observed image, the posterior distribution of the estimated image can be found as a multivariate Gaussian distribution $N(\mathbf{x}|\mu_{\mathbf{x}}, \Sigma_{\mathbf{x}})$ whose parameters are calculated using an iterative procedure [14,23].

The aforementioned algorithm has proven to provide superior performance compared to other state-of-the-art total-variation (TV) minimization algorithms when random Gaussian projection matrices or randomly chosen projection matrices out of the proposed S-cyclic matrix are used [14]. Moreover, the algorithm has proven to be robust to noise, whose variance is estimated. The goal of this paper is to investigate how this performance can be further improved by adaptively selecting projection matrices from the S-cyclic matrix, according to some criterion.

After experimentation with the cyclic matrix, we observed that reconstruction performance can be significantly improved, for low percentages of measurements, when equally spaced projections are used. Here, the equally spaced term refers to the selection of 41×43 masks or rows of the S-matrix. This behavior can be intuitively explained as follows. Each row of the cyclic matrix represents a circular shift of the previous row. Thus, an equally spaced selection of masks corresponds to equally spaced samples in theimage, with spacing equal to the mask selection step. One can visualize this by following the position of a 1 in a row of Φ; in the next acquisition, the location of this 1 has moved vertically in the unstacked image $\mathbf{x}$ by an amount equal to the spacing of the utilized rows in Φ. Such a sampling scheme reassures that pixel information is collected densely over the whole image rather than from only some parts of the image when random projections are used. Furthermore, since PMMW images are assumed to be smooth, neighboring pixels contain similar image intensity information. Hence, the most informative way of sampling would be pixels that are sufficiently separated but at the same time uniformly distributed over the whole image so that most information can be collected when a small percentage of measurements is used. A similar observation has been reported in [24,25], where the authors employ sampling patterns that satisfy probability distributions, such as Poisson disk sampling, jittered sampling ,and farthest point sampling. Such sampling patterns can control gap lengths between sampling points to avoid large local loss of information and result in improved reconstruction quality.

The effect of equally spaced sampling compared to random sampling is presented in Fig. 4. The figure shows how many times each image pixel is sampled when $10\% \simeq 177$ measurements are acquired. One can observe that the equally spaced sampling provides higher density of samples over the whole image, while pixels with a low number of samples are adjacent to pixels with a high number of samples, minimizing the loss of information around their region. Of course, only one instance of the random sampling is presented, since it depends on the particular random selection of the rows of Φ.

A drawback of this method is that equally spaced sampling is valid only for specific percentages, depending on the size of the image. For example, the 41×43 order of our S-matrix does not allow for exact equally spaced selection of matrices when 30% of measurements are required, since, in this case, the

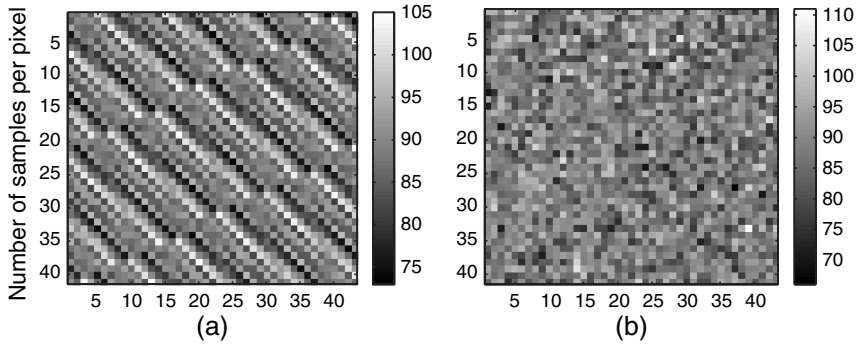

Fig. 4. Comparison of (a) equally spaced sampling to (b) random sampling for $10\% \simeq 177$ measurements out of $N = 1763$.

optimal step of row selection would be 3.33 rows. On the other hand, for 10% of measurements out of the $41 \times 43 = 1763$ pixels of the image (or number of different submasks), only 177 projection matrices (submasks) should be used to acquire the required CS measurements. Based on the equally spaced idea, these projection matrices can be selected starting from the first projection matrix (first row of the 1763×1763 S-cyclic matrix) and then moving by $1763/176 \simeq 10$ rows at a time until all $1 + 176 = 177$ measurements have been obtained. Hence, a natural question arises: "Is there a way to optimally select projection matrices for all possible percentages of measurements?".

Knowing by experimentation that equally spaced sampling gives improved reconstruction, we can start from the exact smaller percentage of measurements that gives an equally spaced solution and then choose the remaining projections optimally. In other words, we want to augment the acquisition matrix, formed by selecting equally spaced rows of Φ, by adding K new rows, where each row is represented by $\mathbf{r}_k$. We can choose these projections by selecting the rows that minimize the differential entropy [26] or maximize $\mathbf{r}_k^T \Sigma_{\mathbf{x}} \mathbf{r}_k$, where $\Sigma_{\mathbf{x}}$ denotes the covariance matrix resulting from the Bayesian reconstruction procedure without the use of the K new rows. Since $\mathbf{r}_k^T \Sigma_{\mathbf{x}} \mathbf{r}_k = \mathrm{Var}(y_k)$, this is equivalent to maximizing the variance of the *expected* measurement y_k. Put differently, the next set of projections $\mathbf{r_k}$ should be selected to constitute the set of measurements $\mathbf{y_k}$ for which the data is most uncertain and, hence, access to the associated measurements would be most informative [26]. Therefore, starting from the closest available equally spaced case, we move to the required percentage by choosing all K most informative measurements in one step. For example, for the collection of $11\% \simeq 194$ measurements, we start from 177 equally spaced projection matrices and we add $K = 17$ new projection matrices based on the described maximum variance rule. The same procedure can be performed sequentially (choosing one new projection at a time), but this method was tested and resulted in slow speeds with almost no improvement in reconstruction quality compared to the one-step selection of all K new projection matrices.

5. Results and Discussion

Experiments have been carried out to demonstrate the effectiveness of our system using the proposed sampling scheme. We use three PMMW images. The first two were acquired without the use of the mask and the integration lens (instead, the first lens is raster scanned in front of the scene to collect a full set of measurements), and the compressed acquisitions are simulated. For the third image, a full set of $41 \times 43 = 1763$ CS observations is obtained with our setup in Fig. 1 and reconstruction is carried out using a subset of them. As a quality metric, we employ the peak signal-to-noise ratio (PSNR), which is directly related to the mean squared error (MSE) as

$$\mathrm{PSNR} = 10 \log_{10}\left(\frac{\max_{\mathbf{x}}^2}{\mathrm{MSE}}\right), \tag{5}$$

$$\mathrm{MSE} = \frac{1}{N}\sum_{i=0}^{N} (\mathbf{x}(i) - \mu_{\mathbf{x}}(i))^2, \tag{6}$$

where $\max_{\mathbf{x}}$ is the maximum possible pixel value of the image (e.g., 255) and $\mu_{\mathbf{x}}$ is the reconstructed image in vector form.

The first two images, for which CS measurements were simulated, depict the middle part of a pair of scissors and a car. The resulting PSNR using random projections and the proposed method is compared in Figs. 5 and 6, for each image respectively, and for percentages 1% to 70% with step 1%. The reconstructed images through our method, corresponding to 10%, 15%, 20%, 25%, and 30% of total observations together with the original PMMW images are also presented in these figures. Additionally, we provide the reconstructed images through random sampling for one of the conducted experiments. This presentation gives the reader an idea of the relation between PSNR and visual quality improvement, which is particularly apparent for percentages 10%–20%.

The equivalent results for the third image, for which CS measurements were obtained through the proposed CS imaging system, are shown in Fig. 7. The image depicts a metallic plate with an open circular hole, having an opaque stripe in the middle. The real PMMW image is unknown in this case. Therefore, we provide a simulation of the real scene [15], and PSNR is compared to the reconstructed image resulting through a full acquisition (100% of measurements).

All the results, simulated (Figs. 5 and 6) and experimental (Fig. 7), agree on the improved performance of the proposed method compared to the usage of random projections, out of the S-cyclic matrix, especially for low percentages of measurements (≤50%). For higher percentages, it is expected that random projections have almost the same performance as the proposed method since a random selection of masks converges to an equally spaced selection of step 2 plus additional random projections in between these selected rows. However, this behavior is not observed in the experimental results (Fig. 7), where improved performance is maintained over the whole range of CS ratios. Certainly, reconstruction performance depends on the image itself. Additional images have been tested, through simulations, and converge to the conclusion that the proposed sampling scheme provides improved reconstruction quality to a lower or higher extent.

Finally, we want to emphasize that the contribution of our proposed sampling scheme is twofold. First, the observation that equally spaced selection of submasks provides superior reconstruction quality is algorithm invariant. That is, any standard CS reconstruction algorithm is expected to exhibit improved performance under the same set of projections. Second, the adaptive selection of additional

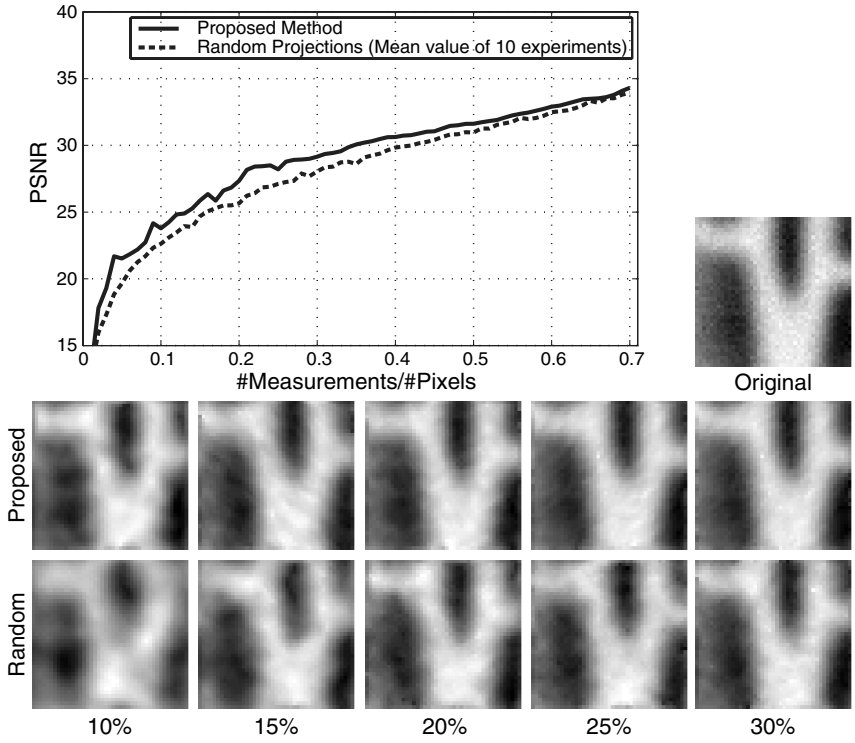

Fig. 5. Simulated CS reconstruction of a PMMW image depicting the middle part of a pair of scissors. PSNR comparison using random projections of the S-cyclic matrix versus the proposed method and example reconstructions for 10%, 15%, 20%, 25%, and 30% of CS measurements.

submasks to reach a required percentage of measurements, which cannot be accommodated by the equally spaced selection scheme, is only covariance dependent. The only requirement is the calculation of the covariance matrix, which is a standard procedure in any Bayesian CS reconstruction algorithm.

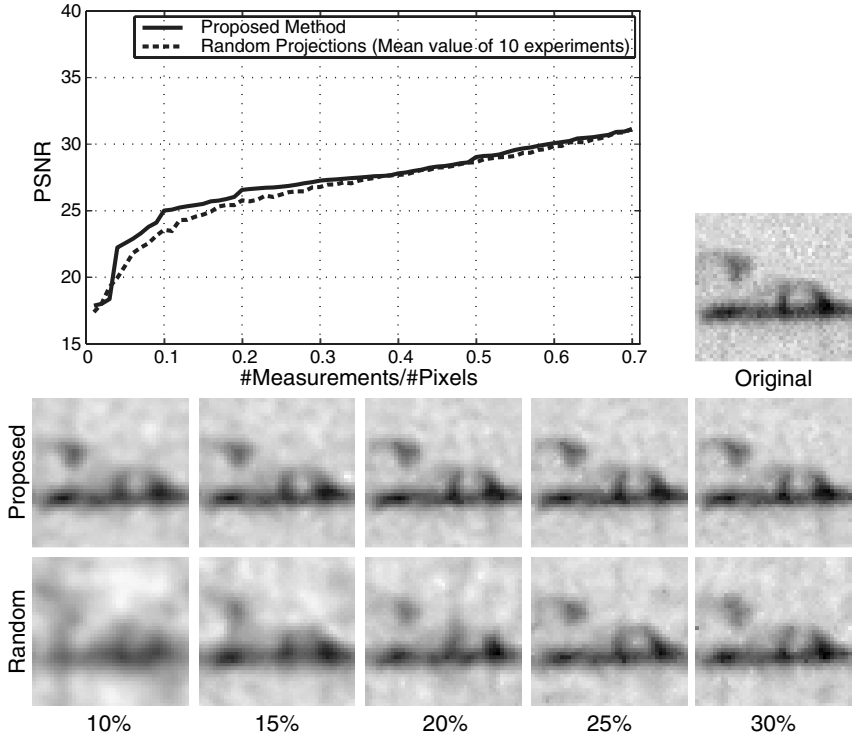

Fig. 6. Simulated CS reconstruction of a PMMW image depicting a car. PSNR comparison using random projections of the S-cyclic matrix versus the proposed method and example reconstructions for 10%, 15%, 20%, 25%, and 30% of CS measurements.

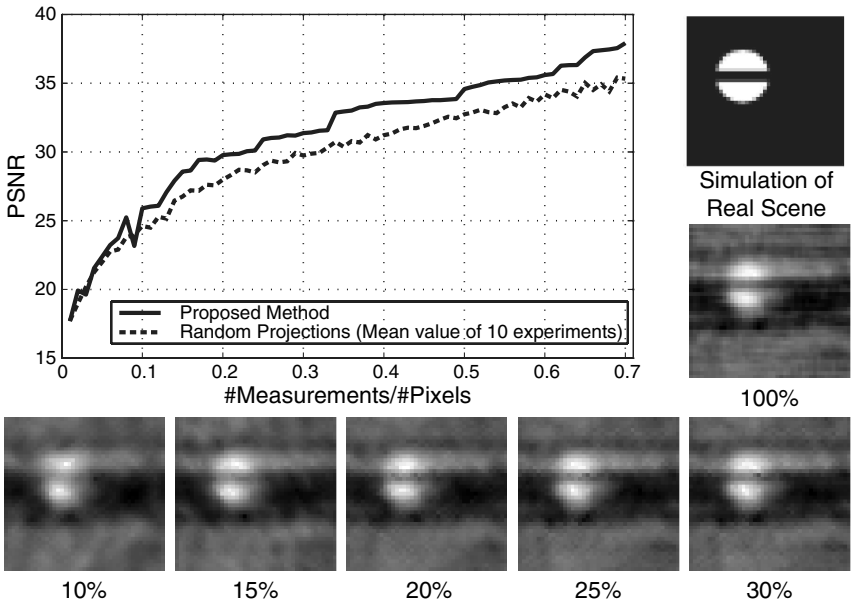

Fig. 7. Experimental CS reconstruction of a PMMW image depicting a metallic plate with an open circular hole, having an opaque stripe in the middle. PSNR comparison using random projections of the S-cyclic matrix versus the proposed method and example reconstructions for 10%, 15%, 20%, 25%, and 30% of CS measurements, through the proposed method. Note, that the real PMMW image is unknown in this case. Therefore, we provide a simulation of the real scene and PSNR is compared to the reconstructed image resulting through a full acquisition (100% of measurements).

For example, the Bayesian reconstruction method presented in [26] could be used instead.

6. Conclusions

To conclude, in this paper we described a single radiometer CS PMMWI system that avoids full raster scanning of the radiometer (or the lens) using a compact mask construction to collect incoherent CS measurements. We mainly proposed a new CS sampling scheme to increase reconstruction quality. The reconstruction algorithm employs a Bayesian CS formulation to estimate the unknown image. Experiments show that the combination of the proposed system with the improved sampling scheme significantly reduces the number of required measurements for acceptable reconstruction.

This research has been supported by a grant from the U.S. Department of Energy and the office of Nonproliferation and Verification Research and Development under the National Nuclear Security Administration. We would also like to thank the Argonne National Laboratory (ANL) for their valuable contribution in constructing the PMMW imager as well as obtaining the images presented in the results section.

References

1. L. Yujiri, M. Shoucri, and P. Moffa, "Passive millimeter-wave imaging," IEEE Microwave Mag. **4**, 39–50 (2003).
2. M. Attia, "Passive millimeter-wave imaging and potential applications in homeland security and aeronautics," presented at Partners in Technology Forum, 21–22 April, 2005.
3. O. Martinez, L. Ferraz, X. Binefa, I. Gomez, and C. Dorronsoro, "Concealed object detection and segmentation over millimetric waves images," in *Proceedings of IEEE Computer Society Conference on Computer Vision and Pattern Recognition Workshops (CVPRW)* (IEEE, 2010), pp. 31–37.
4. M. F. Duarte, M. A. Davenport, D. Takhar, J. N. Laska, T. Sun, K. F. Kelly, and R. G. Baraniuk, "Single-pixel imaging via compressive sampling," IEEE Signal Process. Mag. **25**, 83–91 (2008).
5. Y. Tsaig and D. Donoho, "Compressed sensing," IEEE Trans. Inf. Theory **52**, 1289–1306 (2006).
6. E. J. Candes, J. Romberg, and T. Tao, "Robust uncertainty principles: exact signal reconstruction from highly incomplete frequency information," IEEE Trans. Inf. Theory **52**, 489–509 (2006).
7. R. Fergus, A. Torralba, and W. T. Freeman, "Random lens imaging," Tech. Rep. MIT CSAIL TR 2006-058 (Massachusetts Institute of Technology, 2006).
8. L. McMackin, M. A. Herman, B. Chatterjee, and M. Weldon, "A high-resolution swir camera via compressed sensing," Proc. SPIE **8353**, 835303 (2012).
9. M. A. Neifeld and J. Ke, "Optical architectures for compressive imaging," Appl. Opt. **46**, 5293–5303 (2007).
10. C. F. Cull, D. A. Wikner, J. N. Mait, M. Mattheiss, and D. J. Brady, "Millimeter-wave compressive holography," Appl. Opt. **49**, E67–E82 (2010).
11. C. A. Fernandez, D. Brady, J. N. Mait, and D. A. Wikner, "Sparse Fourier sampling in millimeter-wave compressive holography," in *Digital Holography and Three-Dimensional Imaging* (Optical Society of America, 2010), p. JMA14.
12. I. Noor, O. Furxhi, and E. L. Jacobs, "Compressive sensing for a sub-millimeter-wave single pixel imager," Proc. SPIE **8020**, 8020K (2011).
13. V. M. Patel and J. N. Mait, "Compressive passive millimeter wave imaging with extended depth of field," Opt. Eng. **51**, 091610 (2012).
14. S. Babacan, M. Luessi, L. Spinoulas, A. Katsaggelos, N. Gopalsami, T. Elmer, R. Ahern, S. Liao, and A. Raptis, "Compressive passive millimeter-wave imaging," in *2011 IEEE International Conference on Image Processing (ICIP)* (IEEE, 2011), pp. 2705–2708.
15. N. Gopalsami, T. W. Elmer, S. Liao, R. Ahern, A. Heifetz, A. C. Raptis, M. Luessi, D. Babacan, and A. K. Katsaggelos, "Compressive sampling in passive millimeter-wave imaging," Proc. SPIE **8022**, 80220I (2011).

16. W. L. Chan, K. Charan, D. Takhar, K. F. Kelly, and R. G. Baraniuk, "A single-pixel terahertz imaging system based on compressed sensing," Appl. Phys. Lett. **93**, 121105 (2008).
17. A. Heidari and D. Saeedkia, "A 2D camera design with a single-pixel detector," in *34th International Conference on Infrared, Millimeter, and Terahertz Waves, 2009. IRMMW-THz 2009* (IEEE, 2009), pp. 1–2.
18. M. Harwit and N. J. Sloane, *Hadamard Transform Optics* (Academic, 1979).
19. E. E. Fenimore and T. M. Cannon, "Coded aperture imaging with uniformly redundant arrays," Appl. Opt. **17**, 337–347 (1978).
20. H. D. Lüke and A. Busboom, "Binary arrays with perfect odd-periodic autocorrelation," Appl. Opt. **36**, 6612–6619 (1997).
21. A. Busboom, H. EldersBoll, and H. D. Schotten, "Uniformly redundant arrays," Experimental Astronomy **8**, 97–123 (1998).
22. S. Babacan, R. Molina, and A. Katsaggelos, "Sparse Bayesian image restoration," in *2010 17th IEEE International Conference on Image Processing (ICIP)* (IEEE, 2010), pp. 3577–3580.
23. M. E. Tipping, "Sparse Bayesian learning and the relevance vector machine," J. Mach. Learning Res. **1**, 211–244 (2001).
24. G. Hennenfent and F. J. Herrmann, "Simply denoise: wavefield reconstruction via jittered undersampling," Geophysics, 19–28 (2008).
25. G. Tang, R. Shahidi, and J. Ma, "Design of two-dimensional randomized sampling schemes for curvelet-based sparsity-promoting seismic data recovery," Tech. Rep. TR-2009-03 (UBC Earth and Ocean Sciences Department, 2009).
26. S. Ji, Y. Xue, and L. Carin, "Bayesian compressive sensing," IEEE Trans. Signal Process. **56**, 2346–2356 (2008).